J. Fluid Mech. (1999), *vol.* 400, *pp.* 33–58. Printed in the United Kingdom

Finite-amplitude Taylor-vortex flow of viscoelastic fluids

By ROGER E. KHAYAT

Department of Mechanical & Materials Engineering, The University of Western Ontario, London, Ontario, Canada N6A 5B9
e-mail: Khayat@engga.uwo.ca

(Received 6 February 1996 and in revised form 15 June 1999)

The influence of inertia and elasticity on the onset and stability of Taylor-vortex flow (TVF) is examined for an Oldroyd-B fluid. The Galerkin projection method is used to obtain the departure from Couette flow (CF). Only axisymmetric flow is examined. The solution is capable of capturing the dynamical behaviour observed experimentally for viscoelastic fluids in the inertio-elastic and purely elastic ranges. For flow with dominant inertia, the bifurcation picture is similar to that for a Newtonian fluid. However, transition from CF to TVF is oscillatory because of fluid elasticity. Steady TVF sets in, via supercritical bifurcation, as Re reaches a critical value, Re_c. The critical Reynolds number decreases with fluid elasticity, and is strongly influenced by fluid retardation. As elasticity exceeds a critical level, a subcritical bifurcation emerges at Re_c, similar to that predicted by the Landau–Ginzburg equation. It is found that slip along the axial direction tends to be generally destabilizing. The coherence of the formulation is established under steady and transient conditions through comparison with exact linear stability analysis, experimental measurements, and flow visualization. Good agreement is obtained between theory and the measurements of Muller *et al.* (1993) in the limit of purely elastic overstable TVF.

1. Introduction

While the problem of Taylor–Couette flow (TCF) has been extensively investigated for Newtonian fluids, relatively little attention has been devoted to the case of viscoelastic fluids. Flow instability and turbulence is far less widespread in viscoelastic fluids than in Newtonian fluids because of the high viscosity. Recently, however, there has been a growing interest in the TCF of viscoelastic fluids (see Larson 1992; Shaqfeh 1996 for reviews). Recent linear stability analyses and experiments indicate a dramatic departure in the stability and bifurcation picture of TCF of viscoelastic fluids in comparison with Newtonian fluids. Baumert & Muller (1995, 1999) carried out flow visualization on the TCF of dilute solutions of high-molecular-weight polyisobutylene in oligometric polybutene. Rheological measurements of these solutions confirm that they are of the Boger fluid type (highly elastic with constant viscosity). Using reflective mica platelet seeding, they monitored the transition from the purely azimuthal Couette flow (CF) to the toroidal Taylor-vortex flow (TVF) by varying the shear rate. For a moderately elastic fluid, their experiment suggests that transition can be monotonic or oscillatory with time depending on whether the level of shear rate is low or high. Axially migrating mica alignment bands begin to appear, but band formation ceases with steady vortices setting in after some time. At this point, steady TVF is

observed to persist for a long time (Baumert & Muller 1995). The transition appears to always occur through axisymmetric TVF before wavy vortex flow (WVF) sets in at higher shear rates. This observation was also confirmed recently when the wide-gap flow was examined (Baumert & Muller 1999). However, the absence of a direct transition from CF to WVF is in contradiction with theoretical predictions (Joo & Sahqfeh 1992; Avgousti & Beris 1993; Sureshkumar, Beris & Avgousti 1994), which indicate that non-axisymmetric disturbances are more dangerous than axisymmetric ones. The discrepancy between theory and experiment seems to stem from the type of constitutive model usually adopted in the analyses (Larson, Muller & Shaqfeh 1994); the absence of a distribution of relaxation times in the theoretical constitutive model seems to cancel out the neglect of non-axisymmetric modes in the stability analysis.

For highly elastic (Boger) fluids, normal stress effects (which lead to the Weissenberg rod-climbing phenomenon) prohibit the onset of steady TVF. Only sustained oscillatory TVF is observed for flow with negligible inertia (Muller, Shaqfeh & Larson 1993). The emergence of overstability in the absence of inertia is one of the most interesting phenomena encountered in the TCF of viscoelastic fluids. The existence of such a purely elastic overstable mode was proved through linear stability analysis (Larson, Shaqfeh & Muller 1990) and finite-element calculations (Northey, Armstrong & Brown 1992). Muller *et al.* (1993) conducted laser Doppler velocimetry (LDV) measurements of the axial velocity component of a polyisobutylene-based (Boger) fluid between two concentric cylinders, with the outer cylinder being at rest, and the inner cylinder rotating at constant angular velocity. The measurements show an oscillatory flow at a vanishingly small Reynolds number ($Re \approx 7 \times 10^{-3}$). The flow undergoes a transition from CF to time-periodic TVF as the Deborah number, De, exceeds a critical value, De_c. Here De is the ratio of the relaxation time of the fluid to a typical hydrodynamic time for the problem. The value of De_c is in good agreement with that predicted by earlier linear stability analysis of an Oldroyd-B fluid (Shaqfeh, Muller & Larson 1992). The LDV measurements show that the oscillatory behaviour is not localized but appears to be spread throughout the flow. As De increases from the critical value, the amplitude of oscillation increases like $(De - De_c)^{1/2}$. The corresponding power density spectra show peaks, which are instrumentally sharp at the fundamental frequency, the growth of harmonics, and eventually subharmonics, reflecting, perhaps, the presence of a period-doubling or quasi-periodic motion.

The present paper is a theoretical attempt to (i) reproduce the phenomena observed by Baumert & Muller (1995) on the interplay between inertia and elasticity during the transition from CF to steady TVF, and the flow sequence observed by Muller *et al.* (1993) on purely elastic overstability after the onset of oscillatory TVF; (ii) predict flow behaviour for ranges of flow conditions not covered by experiments; (iii) evaluate the influence of higher-order modes neglected previously (Khayat 1995*c*); and (iv) assess the use of rigid–free and rigid–rigid boundary conditions (Kuhlmann 1985).

The aim is to investigate the onset and stability of finite-amplitude TVF with elastic effects dominating over inertia. It is shown that purely elastic overstability can only be predicted if the higher-order normal stress terms are properly accounted for. These terms were neglected in the previous formulation (Khayat 1995*c*). Particularly, the addition of the azimuthal normal stress component $\tau_{\theta\theta}$ leads to additional coupling with higher-order eigenmodes that cannot be neglected. The resulting nonlinear dynamical system involves sixteen instead of six degrees of freedom. Although more

cumbersome, and therefore less amenable to algebraic manipulations, the present expanded model is more accurate in its predictions, and leads to good agreement with existing formulations and experiments. Additional calculations are also carried out in the absence of inertia, based on a dynamical system that accounts for yet higher-order normal stresses (20NDS), in an attempt to reach a quantitative agreement with the measurements of Muller *et al.* (1993).

A flow sequence similar to that reported by Muller *et al.* (1993) was previously predicted by the six-dimensional nonlinear dynamical system (6NDS) of Khayat (1995*c*). Only a qualitative agreement between theory and experiment was previously possible, as the model is not adequate for the investigation of purely elastic overstability (highly elastic flow). It was found that the presence of inertia, no matter how small it may be, prohibits CF from losing its stability directly to oscillatory TVF (overstable mode). Instead, CF loses its stability first to steady TVF since there is always a finite range of Re values over which steady TVF is stable. A similar sequence of flow was also obtained from the finite-element calculations (with inertia neglected) of Northey *et al.* (1992) for an upper-convected Maxwell (UCM) fluid. These authors, however, report having numerical difficulties in obtaining the solution at the higher Deborah numbers (possibly coinciding with the onset of period doubling). Their calculations are thus limited to an extremely small range of postcritical Deborah numbers.

Recent theoretical work, for axisymmetric and non-axisymmetric flows, has also been examining the linear stability of viscoelastic fluids (Larson *et al.* 1990; Shaqfeh *et al.* 1992; Joo & Shaqfeh 1992), and nonlinear stability as well (Avgousti, Liu & Beris 1993; Avgousti & Beris 1993; Northey *et al.* 1992). New phenomena are constantly being attributed to fluid elasticity (Groisman & Steinberg 1996, 1997). Unlike Newtonian fluids, which obey Newton's law of viscosity, viscoelastic fluids are not governed similarly by a universal constitutive law. The dependence of the predicted flow behaviour on the particular choice of a constitutive model adds another difficulty in our attempt to interpret an already complex flow situation, particularly in the transition and turbulent regimes. Larson (1989) carried out a linear stability analysis in the narrow-gap limit, using the Doi–Edwards and K-BKZ constitutive equations. He found that the dependence of Re_c on De is generally non-monotonic, but the flow is increasingly destabilized by fluid elasticity in the higher De range (Larson 1989).

Similarly to any flow in the transition or turbulent regime, TCF involves a continuous range of excited spatio-temporal scales. In order to assess the effect of the motion of the arbitrarily many smaller length scales, one would have to resolve in detail the motion of the small scales. This issue remains an unresolved one since, despite the great advances in storage and speed of modern computers, it will not be possible to resolve all of the continuous range of length scales in the transition regime. It is by now well established that low-order dynamical systems constitute an alternative to conventional numerical methods as one strives to understand the nonlinear behaviour of flow (Sell, Foias & Temam 1993; Shirer & Wells 1980). These methods are based on the expansion of the flow field in terms of complete sets of orthogonal functions, Fourier series or other standard basis functions. The Galerkin projection method is used, whereby the initial set of partial differential equations is decomposed into an infinite set of ordinary differential equations governing the time-dependent expansion coefficients. The system is then truncated, leading to the finite-dimensional dynamical system. These methods have mainly been applied to Newtonian fluids, and the author appears to be the first to extend their application to non-Newtonian fluids, in thermal

convection (Khayat 1994, 1995*a*, *b*, 1996), rotating flow (Khayat 1995*c*, 1997), and channel flow (Ashrafi & Khayat 1999).

Our earlier work (Khayat 1995*c*) focused on the influence of elasticity and retardation on the stability and amplitude of the Taylor vortices with inertia dominating the flow. A truncated Fourier representation with Galerkin projection of the flow field similar to that of Kuhlmann and associates for a Newtonian fluid was proposed. Kuhlmann (1985), and later Kuhlmann, Roth & Lücke (1988) examined the stationary and time-periodic TVF, in the narrow-gap limit and for arbitrary gap width, respectively, with the inner cylinder rotating at constant and harmonically modulated angular velocity. The solution to the full Navier–Stokes equations was obtained by implementing a finite-difference scheme, and the approximate approach based on the Galerkin projection. Comparison of flows based on the two methods led to good agreement. Since elastic effects in Khayat (1995*c*) were assumed to be weak, higher-order normal stress terms were neglected, thus leading to a six-dimensional nonlinear system (6NDS), and reducing to Kuhlmann's three-dimensional system (3NDS) for a Newtonian fluid (Khayat 1995*c*). While the two models suffer from a similar level of truncation, the addition of the viscoelastic effect, even to a very weak extent, appears to alter dramatically the stability and bifurcation picture. Most importantly, elasticity tends to destabilize the TVF, leading to chaotic behaviour and the emergence of a Lorenz type attractor. As the Deborah number increases, the onset of TVF occurs at a Reynolds number that decreases with De. Beyond a critical De value, the exchange of stability takes place via a subcritical instead of a supercritical bifurcation. Since the previous formulation (Khayat 1995*c*) is not adequate for flow with dominant elastic effects, most results from existing linear analyses, finite-amplitude numerical calculations, and experiments on the purely elastic overstability could not be recovered.

The paper is organized as follows. In § 2, the derivation of the nonlinear dynamical system is discussed. The steady-state solutions and their stability are examined in § 3. The influence of inertia for weakly and strongly elastic flows is examined in § 4, as well as comparison between theory and experiment. Discussion and concluding remarks are covered in § 5.

2. Problem formulation and solution procedure

Consider an incompressible viscoelastic fluid of density ρ, relaxation time λ and viscosity η. In this study, only fluids that can be reasonably represented by a single relaxation time and constant viscosity are considered. The fluid is confined between two infinite and concentric cylinders of inner and outer radii R_i and R_o, respectively. The flow is assumed to be axisymmetric. The inner cylinder is taken to rotate at an angular velocity Ω, while the outer cylinder is at rest. Typically, the fluid examined is a polymer solution composed of a Newtonian solvent and a polymer solute of viscosities η_s and η_p, respectively. Thus, $\eta = \eta_s + \eta_p$.

2.1. *General equations and boundary conditions*

The conservation of mass and linear momentum equations may be, respectively, written as

$$\nabla \cdot \boldsymbol{U} = 0, \quad \rho \left(\frac{\partial \boldsymbol{U}}{\partial T} + \boldsymbol{U} \nabla \cdot \boldsymbol{U} \right) = -\nabla P + \eta_s \nabla^2 \boldsymbol{U} + \nabla \cdot \boldsymbol{T}, \tag{1}$$

where ∇ is the gradient operator, T is the time, $\boldsymbol{U}$ is the velocity vector and $\boldsymbol{T}$ is the elastic part of the deviatoric stress tensor in the (R, Θ, Z) system. In this work, the fluid is assumed to obey the Oldroyd-B constitutive model (Bird, Armstrong & Hassager 1987) so that $\boldsymbol{T}$ is governed by the following equation:

$$\lambda \left[\frac{\partial \boldsymbol{T}}{\partial T} + \boldsymbol{U} \cdot \nabla \boldsymbol{T} - (\nabla \boldsymbol{U})^t \cdot \boldsymbol{T} - \boldsymbol{T} \cdot \nabla \boldsymbol{U} \right] = -\boldsymbol{T} + \eta_p \left[\nabla \boldsymbol{U} + (\nabla \boldsymbol{U})^t \right]. \tag{2}$$

The boundary conditions on the cylinder walls are prescribed as follows. Regardless of the nature of the two cylinders, the no-penetration condition must apply at any time. Rigid (stick) conditions are assumed to hold on the walls in the azimuthal direction. Along the axial direction, rigid (stick) or free (slip) conditions can be assumed, leading, respectively, to the rigid–rigid (RR) or rigid–free (RF) boundary conditions for the problem. The introduction of the RF conditions is customary for Newtonian flows (Kuhlmann 1985; Kuhlmann *et al.* 1988), and should be compared to the free-surface assumption usually adopted in the Rayleigh–Bénard convection problem (Shirer & Wells 1980; Veronis 1966; Drazin & Reid 1981; McLaughlin & Martin 1975). This is equivalent to having the cylinders lubricated along the axial direction. In thermal convection, both the lower and upper planes, which are separated by the fluid, are assumed to be free surfaces. This is not a realistic assumption, but it makes the problem formulation much easier to handle since trigonometric rather than hyperbolic (Chandrasekhar) functions can be used in the expansion of the solution along the gap.

For TCF, a slip along the Z-direction precipitates the onset of Taylor vortices given the absence of axial friction. In the narrow-gap limit, linear stability analysis for a Newtonian fluid gives the minimum value of the critical $Re_c(k)$ and corresponding wavenumber, k_m, for the onset of TVF, respectively, as $Re_c^m = 41.2/\sqrt{\varepsilon}$ and $k_m = 3.12$ if RR conditions are assumed (McLaughlin & Martin 1975), and $Re_c^m = 25.6/\sqrt{\varepsilon}$ and $k_m = 2.23$ (Kuhlmann 1985) if RF conditions are used. The neutral stability curves in both cases are qualitatively similar. While RR conditions tend to give more accurate values for Re_c^m and k_m, RF conditions lead to a torque value at the onset of TVF that is much closer to what existing formulations predict (Kuhlmann 1985; Kuhlmann *et al.* 1988; Davey 1962; Stuart 1958). As to the nonlinear range, both RR and RF conditions have been used with the same level of truncation (Kuhlmann 1985). The two models lead essentially to the same qualitative behaviour. Based on these arguments, one may then suspect that a similar conclusion can be drawn in the case of a viscoelastic fluid. This is indeed confirmed in the present study through comparisons with existing linear stability analysis results, experimental measurements and flow visualization. Aside from giving a more accurate torque estimate at the onset of TVF, RF conditions lead to equations that reduce to the 6NDS studied earlier (Khayat 1995*c*), thus allowing the examination of the influence of the higher-order modes neglected previously. These equations, in turn, reduce further to the Lorenz system for a Newtonian fluid, a system extensively investigated in the past thirty years or so (Sparrow 1983).

2.2. *Governing equations in the narrow-gap limit*

Consider the flow between two concentric cylinders in the limit when the radius R_i/R_o is very close to 1. Suitable scales are sought for length, time, velocity and

stress as follows:

$$\left.\begin{aligned} &x = \frac{R - R_i}{d}, \quad z = \frac{Z}{d}, \quad t = \frac{R_i\Omega}{d}T, \\ &(u_x, u_z) = \frac{1}{R_i\Omega}(U_R, U_Z), \quad u_y = \frac{U_\Theta}{R_i\Omega\sqrt{\varepsilon}}, \quad (\tau_{xx}, \tau_{zz}, \tau_{xz}) = \frac{d}{\eta R_i\Omega}(T_{RR}, T_{ZZ}, T_{RZ}), \\ &p = \frac{d}{\eta R_i\Omega}P, \quad (\tau_{xy}, \tau_{zy}) = \frac{d}{\eta R_i\Omega\sqrt{\varepsilon}}(T_{R\Theta}, T_{Z\Theta}), \quad \tau_{yy} = \frac{d}{\varepsilon\eta R_i\Omega}T_{\Theta\Theta}. \end{aligned}\right\} \tag{3}$$

Substitution of expressions (3) into (1) and (2) leads to important dimensionless groups in the problem, namely the Reynolds number, Re, the Deborah number, De, the solvent-to-solute viscosity ratio, Rv, and gap-to-radius ratio, ε:

$$Re = \frac{R_i\Omega d}{v}, \quad De = \frac{\lambda R_i\Omega}{d}, \quad Rv = \frac{\eta_s}{\eta_p}, \quad \varepsilon = \frac{d}{R_i}, \tag{4}$$

where $v = \eta/\rho$ is the kinematic viscosity of the fluid solution. Another important group, the Elasticity number, $E = De/Re = \lambda v/d^2$, will also be used. Unlike De, E depends only on the properties of the fluid. The equations governing the departure from the CF are then derived by expanding the flow field in powers of ε, and excluding terms of $O(\varepsilon)$ and higher. Thus, the continuity and momentum conservation equations reduce to

$$u_{x,x} + u_{z,z} = 0, \tag{5}$$

$$Re\lfloor u_{x,t} + u_x u_{x,x} + u_z u_{x,z} - u_y^2 - 2(1-x)u_y \rfloor = \tau_{xx,x} + \tau_{xz,z} - \tau_{yy} - p_{,x} + aRv(u_{x,xx} + u_{x,zz}), \tag{6}$$

$$Re(u_{y,t} + u_x u_{y,x} + u_z u_{y,z} - u_x) = \tau_{xy,x} + \tau_{zy,z} + aRv(u_{y,xx} + u_{y,zz}), \tag{7}$$

$$Re(u_{z,t} + u_x u_{z,x} + u_z u_{z,z}) = \tau_{xz,x} + \tau_{zz,z} - p_{,z} + aRv(u_{z,xx} + u_{z,zz}), \tag{8}$$

whereas the constitutive equation (2) leads to

$$De[\tau_{xx,t} + u_x\tau_{xx,x} + u_z\tau_{xx,z} - 2(u_{x,x}\tau_{xx} + u_{x,z}\tau_{xz})] = -\tau_{xx} + 2au_{x,x}, \tag{9}$$

$$De\{\tau_{yy,t} + u_x\tau_{yy,x} + u_z\tau_{yy,z} - 2\lfloor(u_{y,x} - 1)\tau_{xy} + au_{y,x} + u_{y,z}\tau_{yz}\rfloor\} = -\tau_{yy}, \tag{10}$$

$$De[\tau_{zz,t} + u_x\tau_{zz,x} + u_z\tau_{zz,z} - 2(u_{z,x}\tau_{xz} + u_{z,z}\tau_{zz})] = -\tau_{zz} + 2au_{z,z}, \tag{11}$$

$$De\{\tau_{xy,t} + u_x\tau_{xy,x} + u_z\tau_{xy,z} - \lfloor u_{x,x}(\tau_{xy} + a) + u_{x,z}\tau_{yz} + (u_{y,x} - 1)\tau_{xx} + u_{y,z}\tau_{xz}\rfloor\} = -\tau_{xy} + au_{y,x}, \tag{12}$$

$$De[\tau_{xz,t} + u_x\tau_{xz,x} + u_z\tau_{xz,z} - (u_{z,x}\tau_{xx} + u_{x,z}\tau_{zz})] = -\tau_{xz} + a(u_{x,z} + u_{z,x}), \tag{13}$$

$$De\{\tau_{yz,t} + u_x\tau_{yz,x} + u_z\tau_{yz,z} - \lfloor u_{z,x}(\tau_{xy} + a) + u_{z,z}\tau_{yz} + (u_{y,x} - 1)\tau_{xz} + u_{y,z}\tau_{zz}\rfloor\} = -\tau_{yz} + au_{y,z}, \tag{14}$$

where a comma denotes partial differentiation, and $a = 1/(Rv + 1) = \eta_p/\eta$ is the polymer-to-solution viscosity ratio.

2.3. *Solution procedure*

The solution of (1) and (2) is carried out using the Galerkin projection method. The variables $u_i(x,z,t)$, $p(x,z,t)$ and $\tau_{ij}(x,z,t)$ are represented by infinite Fourier series of fundamental wavelength π/k (in units of d) in the z-direction, and complete sets of orthogonal functions satisfying the boundary conditions in the x-direction. After elimination of the pressure in the momentum equations, the flow variables can be written as spectral sums:

$$u_i(x,z,t) = \sum_{m,n} u_i^{mn}(t) e^{imkz} f_i^n(x), \quad \tau_{ij}(x,z,t) = \sum_{m,n} \tau_{ij}^{mn}(t) e^{imkz} g_{ij}^n(x), \tag{15}$$

where $f_i^n(x)$ and $g_{ij}^n(x)$ are trigonometric or Chandrasekhar (1961) functions depending on whether the RF or the RR boundary conditions are used, respectively. The number of modes is reduced by invoking the symmetry allowed by equations (1) and (2) as the flow is invariant under $z \to -z$, and $u_z \to -u_z$, $\tau_{\alpha z} \to -\tau_{\alpha z}$ ($\alpha = x, y$). This amounts to having invariance in the flow when the Taylor–Couette apparatus is turned upside down (Marcus 1984).

A suitable level of truncation is imposed that leads to the final nonlinear dynamical system. A judicious selection process is applied for the choice of the various modes in order to ensure the physical and mathematical coherence of the final model. Based on the comparisons with the exact results from linear stability analysis and experiment, only two fundamental modes in the z-direction and two modes in the x-direction appear to be sufficient to capture qualitatively most of the experimental observations of Baumert & Muller (1995) on the influence of inertia. This truncation level leads to a 16-dimensional nonlinear dynamical system (16NDS), where zeroth-order modes have been neglected except for u_y and τ_{xy}. The modal representations for the RF and the RR formulations are given in Appendices A and B, respectively. In the absence of inertia, additional terms in the normal stress components turned out to be needed, leading to a 20NDS model where the zeroth-order modes are included for all stress components (Khayat 1997). As will be seen below, the inclusion of more modes in the normal stress components appears to be crucial for good quantitative agreement with the experimental measurements of Muller *et al.* (1993) to be reached.

3. Linear stability analysis

In this section the linear stability of the CF and the TVF are examined. For small values of E (or De) and Rv, inertia effect is important, and one expects the stability picture to be similar to that of a Newtonian fluid. In this case, flow stability is monitored by increasing inertia for a fluid of a fixed level of elasticity. As E increases, the stability picture changes, giving rise to a periodic solution, or overstability, which is the result of normal stress effects.

3.1. *Stability of the Couette flow*

Although the emphasis will be on the influence of inertia on the stability of a viscoelastic fluid, it is helpful to start with the stability of a purely elastic fluid as an exact solution is easier to obtain for the eigenvalue problem. For an upper-convected Maxwell (UCM) fluid ($Rv = 0$), the eigenvalue of the problem may be written as $\Lambda = 2\varepsilon De^2/k(1-i\omega De)^2$, where ω is the complex frequency (Larson *et al.* 1990). There is an exact solution of the eigenvalue problem for both the RR and RF conditions, which is obtained using the direct method. The eigenvalue Λ is found to be imaginary,

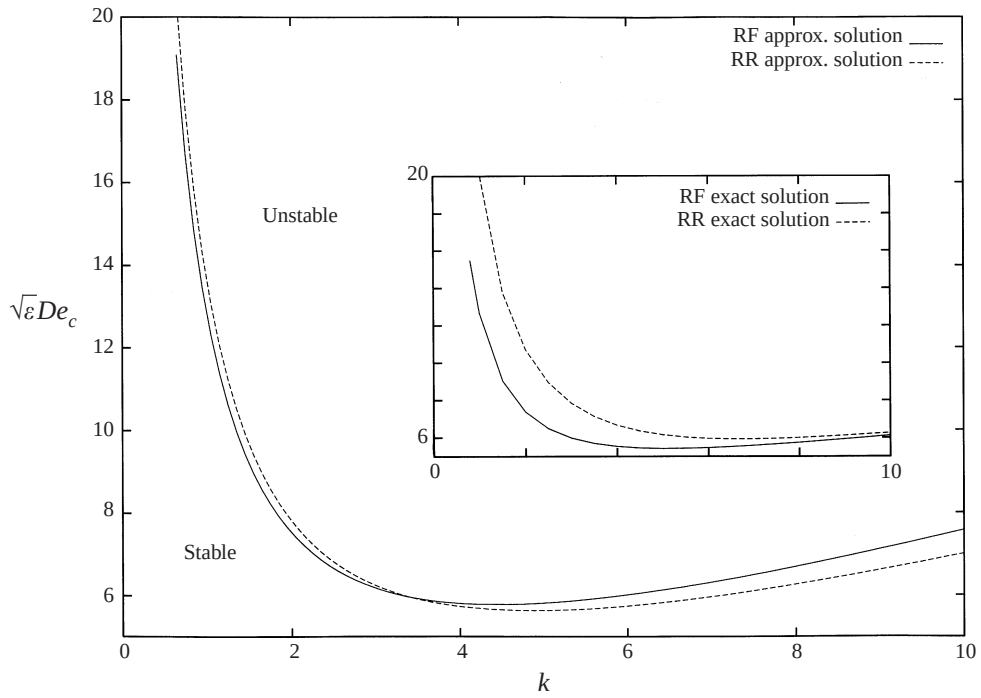

FIGURE 1. Influence of boundary conditions and comparison between approximate and exact neutral stability for the onset of purely elastic oscillatory TVF. Marginal curves for a UCM fluid ($Rv = 0$). Note that the inset shows the exact marginal curves.

leading to the same dispersion relation as that of Larson *et al.* (1990). The exact minimum critical Deborah number $De_c^m = De_c(k = k_m)$ and corresponding wavenumber, k_m, for the onset of the most unstable (overstable) mode are, respectively, $De_c^m = 5.77/\sqrt{\varepsilon}$ and $k_m = 4.44$ for the RF conditions, compared to $5.92/\sqrt{\varepsilon}$ and 6.7 for the RR conditions. Here $De_c(k)$ is the critical Deborah number, for a given k, at which oscillatory TVF (overstability) sets in. The exact solution to the eigenvalue problem gives an estimate of the magnitude of the error resulting from the truncation in solution. One should expect that the error remains of the same order when such a truncation is applied to the solution of the full nonlinear equations for small departure from CF. Figure 1 shows the exact neutral stability curves based on the RF and RR conditions, the latter being the same as the exact solution of Larson *et al.* (1990), and the corresponding approximate curves. All four marginal curves exhibit similar behaviour. At small k, De_c decreases sharply with k, reaches a minimum at $k = k_m$, and increases again for $k > k_m$. All curves indicate a general flattening around k_m, confirming the experimentally observed wide range of wavenumbers for which overstability sets in (Baumert & Muller 1995; Larson 1992). The figure indicates a close quantitative agreement between the exact and approximate solutions for $k < k_m$. This holds for both the RF and RR conditions. As to the influence of boundary conditions, the figure shows that the type of boundary conditions is more influential at small wavenumber. The qualitative behaviour is, however, the same regardless of the type of boundary conditions used.

In the presence of inertia, Joo & Shaqfeh (1992) carried out the numerical solution of the linear stability problem using the RR boundary conditions, and examined the

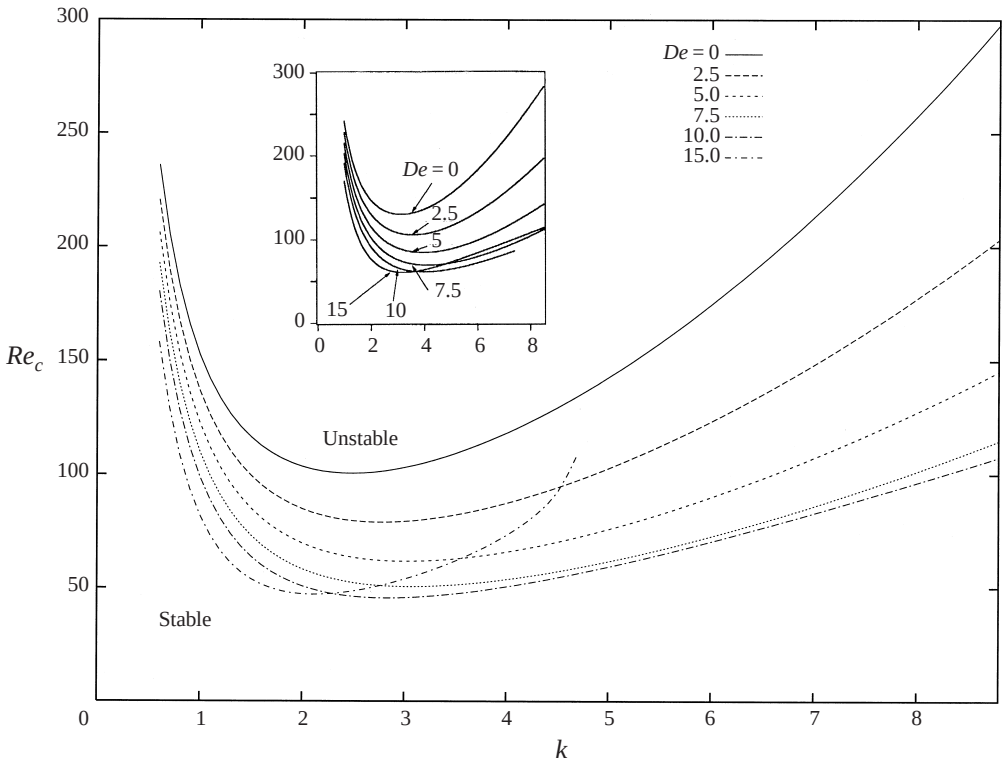

FIGURE 2. Influence of fluid elasticity and marginal stability curves for a UCM fluid ($Rv = 0$) based on the RR boundary conditions and $\varepsilon = 0.01$. The results of Joo & Shaqfeh (1992) are included in the inset.

influence of elasticity for a UCM fluid. Figure 2 displays the neutral stability curves in the (Re, k)-plane for the onset of steady TVF for $0 \leqslant De \leqslant 15$ and $\varepsilon = 0.1$. Again, let $Re_c(k, De)$ be the critical Reynolds number at given k and De. The exact results of Joo & Shaqfeh are included in the inset, which compare well with the curves based on the 16NDS model. For all De values, $Re_c(k, De)$ decreases roughly like $1/k^2$ near $k = 0$, reaches a minimum, $Re_c^m(De)$, at $k = k_m$, and then increases roughly like k^2 for large k. There is a shift in the value of k_m towards the right as De increases, thus reflecting the greater difficulty in observing axisymmetric Taylor vortices in the case of highly elastic fluids. On the other hand, this minimum becomes less localized with increasing fluid elasticity, resulting in a wider range of wavenumbers at which Taylor vortices set in. However, for $De > 10$, the neutral curves show again a very localized minimum, with an increasingly narrower range of wavenumbers for CF to lose its stability to steady TVF. For a given k value, Re_c decreases generally with De roughly like $1/De$. This is, perhaps, the most important result in figure 2: fluid elasticity tends to precipitate the onset of axisymmetric Taylor vortices at any value of the wavenumber in the axial direction.

3.2. *Stability of the Taylor-vortex flow and bifurcation*

For $E < E^{sub}$, there is an exchange of stability, similar to the Newtonian case, between the origin (CF) and the two branches C_1 and C_2 (steady TVF) via a supercritical bifurcation at $Re = Re_c(E, Rv, k)$. As was established above, Re_c becomes increasingly smaller as E increases. For $E > E^{sub}$, the bifurcation is subcritical. In both regimes, as

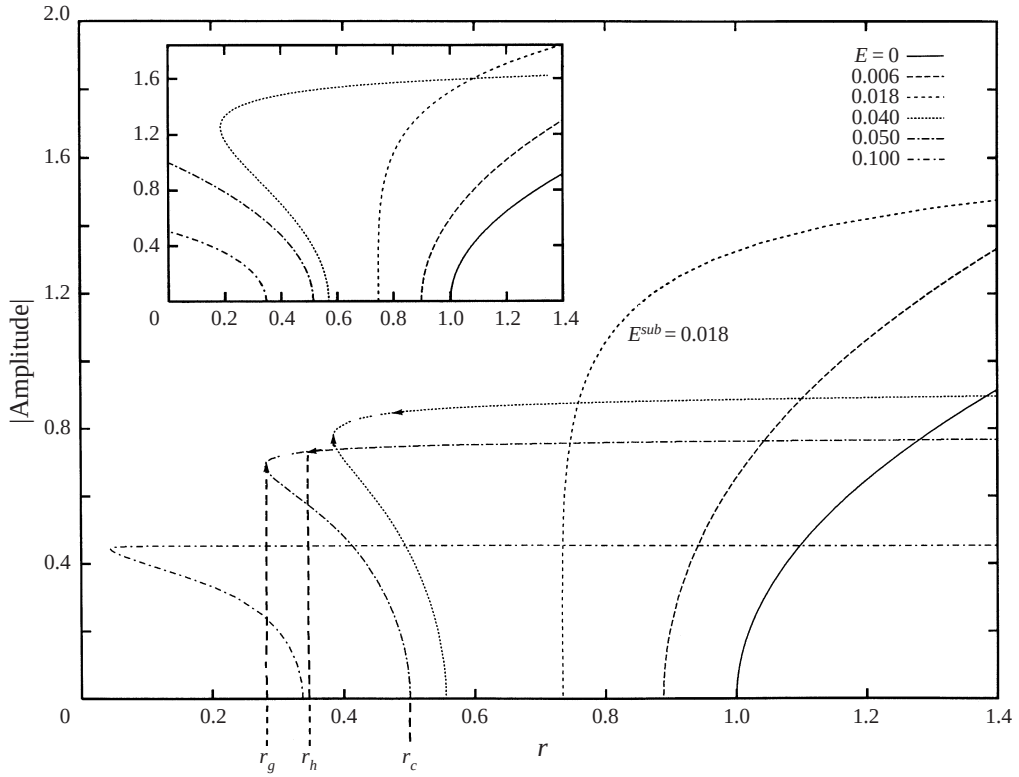

FIGURE 3. Bifurcation diagrams and influence of higher-order modes for a UCM fluid ($Rv = 0$) with $k = 3$ and $\varepsilon = 0.01$. Steady-state solutions are plotted against the normalized Reynolds number: $r(k) = Re/Re_c^{Newt}(k)$, where $Re_c^{Newt}(k)$ is the critical Reynolds number for the onset of TVF for a Newtonian fluid. Super- and subcritical bifurcations for weakly and strongly elastic flows corresponding, respectively, to $E < E^{sub}$ and $E > E^{sub}$. For the subcritical curves, the stable regions are indicated by breaks in the curves and are delimited by two arrows. Inset shows bifurcation diagrams based on lower-order theory (6NDS of Khayat 1995*c*) with $E^{sub} = 0.014$.

Re increases and reaches a second critical value $Re_h(E, Rv, k)$, the branches C_1 and C_2 lose their stability in turn via a Hopf bifurcation. This bifurcation and stability picture has already been established on the basis of the 6NDS mode (Khayat 1995*c*) and is next confirmed when higher-order modes (16NDS) are included.

The influence of fluid elasticity on the bifurcating branches at $Re = Re_c$ is depicted in figure 3 for a UCM fluid ($Rv = 0$) and $k = 3$. These curves correspond to the RF formulation, and are compared with the bifurcation diagrams from Khayat (1995*c*) included in the inset. Because of symmetry with respect to the Re-axis, only one set of branches (C_1) is shown. There are several important aspects to be observed from figure 3 and the inset therein. The first is that there is a strong dependence of Re_c on fluid elasticity. For small E, there is a supercritical bifurcation at $Re = Re_c$, with Re_c becoming increasingly smaller as E increases, and decreasing all the way to zero. At the critical value $E = E^{sub}(Rv, k)$, which in this case is equal to 0.018, the bifurcation changes from super- to subcritical. In the supercritical regime, when $Re < Re_c$, a small disturbance of the base flow decays exponentially according to linear stability theory. As Re exceeds Re_c, linear stability theory predicts exponential growth of a small disturbance from CF. This growth is, however, halted by the stabilizing nonlinear effects.

In the subcritical regime ($E > E^{sub}$), when $Re < Re_g$ (shown here for the curve $E = 0.05$), the base flow is globally asymptotically stable (Drazin & Reid 1981). When $Re_g < Re < Re_c$, two solutions exist for the disturbance from the CF for the C_1 branch. In this case, any disturbance below a certain threshold decays to the origin (CF). Above the threshold value, the CF is destabilized. In this range of Re values, the flow is commonly defined as metastable (Normand & Pomeau 1977). Whether the bifurcation at Re_c is subcritical or supercritical, the TVF loses its stability at some critical $Re = Re_h > Re_c$ (shown here for the curve $E = 0.05$). This second bifurcation is absent for Newtonian fluids. Thus, the presence of fluid elasticity appears to be a sufficient condition for the loss of stability of TVF. Indeed, at $Re = Re_h(E, Rv, k) > Re_c$, linear stability analysis around C_1 and C_2 indicates that these two branches lose their stability via a Hopf bifurcation. In figure 3, the range of Re values for which the branch C_1 is stable (for $E > E^{sub}$) is indicated by breaks in the lines between two arrows. It is observed from the figure that, for highly elastic fluids ($E > 1$), the range of stability of the C_1 (and C_2) decreases essentially to zero, so that the (steady) TVF is unstable for any postcritical Re value.

4. Finite-amplitude TVF and comparison with experiment

The influence of inertia and elasticity on weakly and strongly elastic flows is examined in some detail, including purely elastic (zero inertia) flow. A weakly (strongly) elastic flow is defined as one with $E < E^{sub}$ ($E > E^{sub}$) for the exchange of stability between CF and TVF to occur via a supercritical (subcritical) bifurcation. Comparison is carried out between theory and the experiments of Baumert & Muller (1995) and Muller *et al.* (1993). The results are also compared with the numerical calculations of Avgousti *et al.* (1993) whenever possible.

4.1. *Influence of inertia on weakly elastic flow*

Consider the transition of weakly elastic flow as the shear rate (measured by De) is increased. The aim of the present calculations is to reproduce some of the experimental observations of Baumert & Muller (1995) as the CF loses its stability to TVF, and predict what may happen for the range of higher shear rate not covered by experiment. Given the uncertainty in the experimental values of the relaxation time, λ, and the wavenumber, k, and the assumptions adopted in the derivation of the low-dimensional dynamical system, only a qualitative agreement can be expected. The influence of inertia on a moderately weakly elastic Oldroyd-B fluid is examined by fixing E and varying De (or, equivalently, varying Re). The case of a fluid with $E = 0.16$ is considered, which corresponds roughly to the low-viscosity Boger fluid used by Baumert & Muller (1995), with $\rho = 0.856\,\mathrm{g\,cm^{-3}}$, $\eta_s = 2.6\,\mathrm{P}$ and $\eta = 3.0\,\mathrm{P}$. The experimental relaxation time was found to be equal to $\lambda = \lambda_s = 0.021\,\mathrm{s}$ or $\lambda_t = 0.11\,\mathrm{s}$ ($E_s = 0.164$ or $E_t = 0.94$), depending, respectively, on whether steady shear or transient measurement was used. The value of the viscosity ratio is $Rv = 6.5$. Figure 4 shows the time evolution of the (dimensional) axial velocity component U_z midway through the gap. The evolution of the velocity is displayed for $13 < De < 14$ ($81.25 < Re < 87.5$), above the critical shear rate, $De_c \approx 13$ ($Re_c \approx 81.25$). The curves in the figure are similar to the results reported in figure 1 of Avgousti *et al.* (1993), and the trend is in agreement with the observations of Baumert & Muller (1995) for low- and medium-viscosity fluids. The initial condition taken for all the curves in figure 4 corresponds to a slight perturbation form CF.

Typically, the flow evolves monotonically from CF to steady TVF over a period of

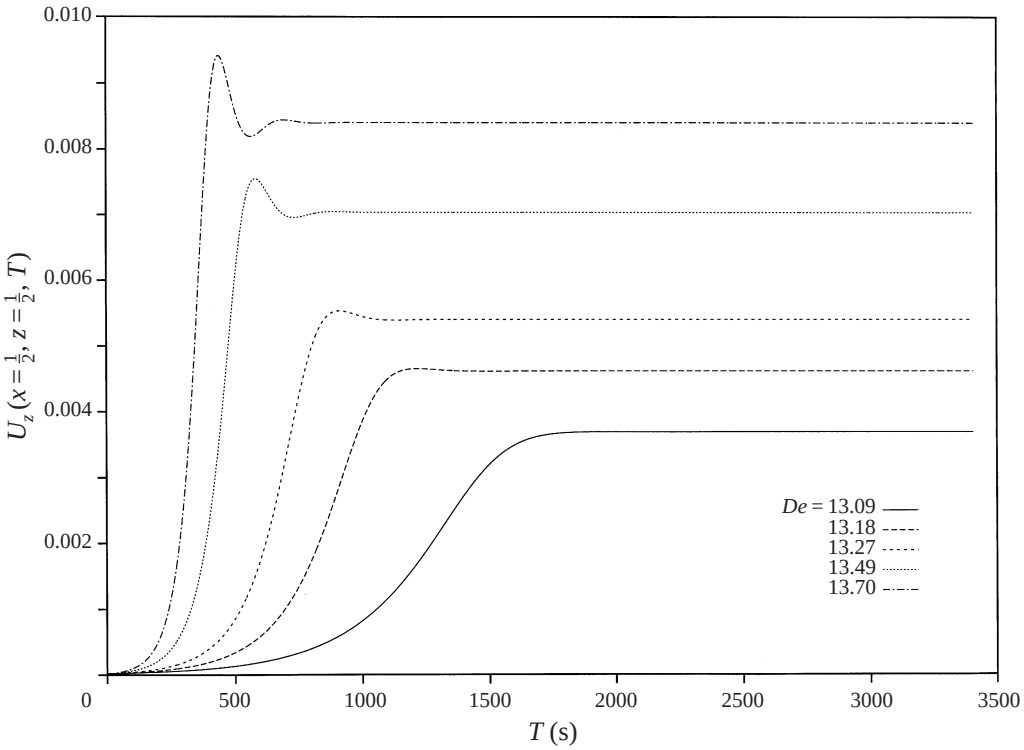

FIGURE 4. Monotonic time evolution of the axial velocity for different shear rates ($13 < De < 14$) and small initial perturbation of the base flow ($E = 0.16$, $Rv = 6.5$, $k = 3.5$ and $\varepsilon = 0.093$).

time, $T_{CF/TVF}$, which decreases with increasing shear rate as depicted from figure 4. This behaviour is in agreement with the measurements of Baumert & Muller (1995). Figure 5 displays the time after shear initiation of the appearance of steady vortices as a function of De (shear rate). An inset showing the values from experiment (for $E_s = 44$) is also included for comparison, and reveals good qualitative agreement with theoretical predictions. At higher shear rates, theory predicts that $T_{CF/TVF}$ begins to increase with De. This is depicted in figure 4 for the curves corresponding to $De > 13.2$, which show a local depression in the flow amplitude before steady TVF sets in. In fact, as De is further increased, oscillatory behaviour emerges before the onset of steady TVF as shown in figure 6 for $17 < De < 18$. The secondary flow gains strength initially at a much faster rate than for the lower range of shear rates (figure 4). The amplitude of oscillation decays with time until the onset of steady TVF, but the frequency appears to remain constant. As De increases, the overall amplitude of oscillation increases, and is accompanied by a phase shift and delay in the onset of steady TVF. Eventually, oscillatory behaviour is sustained for longer time for higher De values. In the limit, no steady TVF is found.

Consider now the influence of the initial conditions on the ensuing flow behaviour. Baumert & Muller (1995) report that 'flow behaviour was not found to be particularly sensitive to the type of velocity ramp imposed' initially. This observation is confirmed here by taking as initial conditions the steady TVF reached before increasing the shear rate, instead of starting again from near CF as in figures 4 and 6. The resulting sequence of initial flow transients is depicted in figure 7 for the range $16 < De < 21$. The figure displays the evolution of flow over a period of 54 000 s, subdivided into

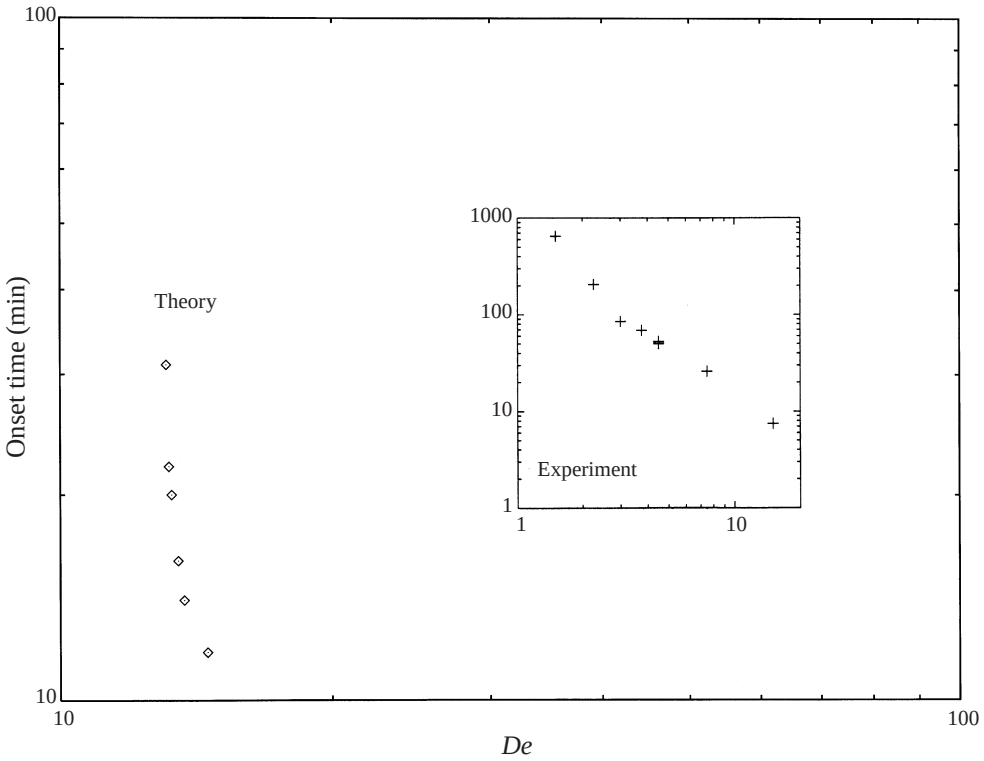

FIGURE 5. Time after shear initiation of the appearance of steady vortices as a function of the shear rate (De). The values in the figure are based on the curves in figure 4. The inset shows the experimental measurements of Baumart & Muller (1995) for a medium viscosity fluid.

three equal periods of 18 000 s. The first segment is shown in figure 7(*a*) for the range of shear rates corresponding to $16 < De < 19$. Comparison between the curves in figure 6 and those in figure 7(*a*) indicates that the flow behaviour is essentially unaffected by initial conditions. It is interesting to note the similarity in the emergence and decay of oscillatory behaviour between one steady level and the other. The figure clearly shows that the time that steady TVF takes to set in increases with shear rate. This is a result of the oscillatory transition that takes a longer time for the higher shear rate. This is indeed even more evident from figure 7(*b*), which shows, for the range $18 < De < 20$, that steady TVF does not even set in over the time period over which the shear rate is applied. The oscillations tend to decay at a slower rate as De increases, and eventually start to grow with time as indicated in the last portion of figure 7(*b*), corresponding to $De = 19.26$. This growth, which is linear upon onset, does not remain unstable over time as linear stability analysis suggests. At some time, when the signal amplitude is large enough, nonlinear effects become significant and halt the (exponential) growth. The bifurcation diagrams in figure 3 suggest that steady TVF is possible as long as De (or Re) is below $De_h(E, Rv, k)$ (or Re_h). This corresponds to the onset of a Hopf bifurcation at $De = De_h$ when steady TVF becomes periodic. For the present flow in figure 7, De_h is found to be approximately equal to 19.

In figures 7(*a*) and 7(*b*), and for the range $16 < De < 19.15$, the computation is limited to flow with final state that corresponds to a standing wave (steady TVF). This also corresponds to most of the range of shear rates examined in the experiment

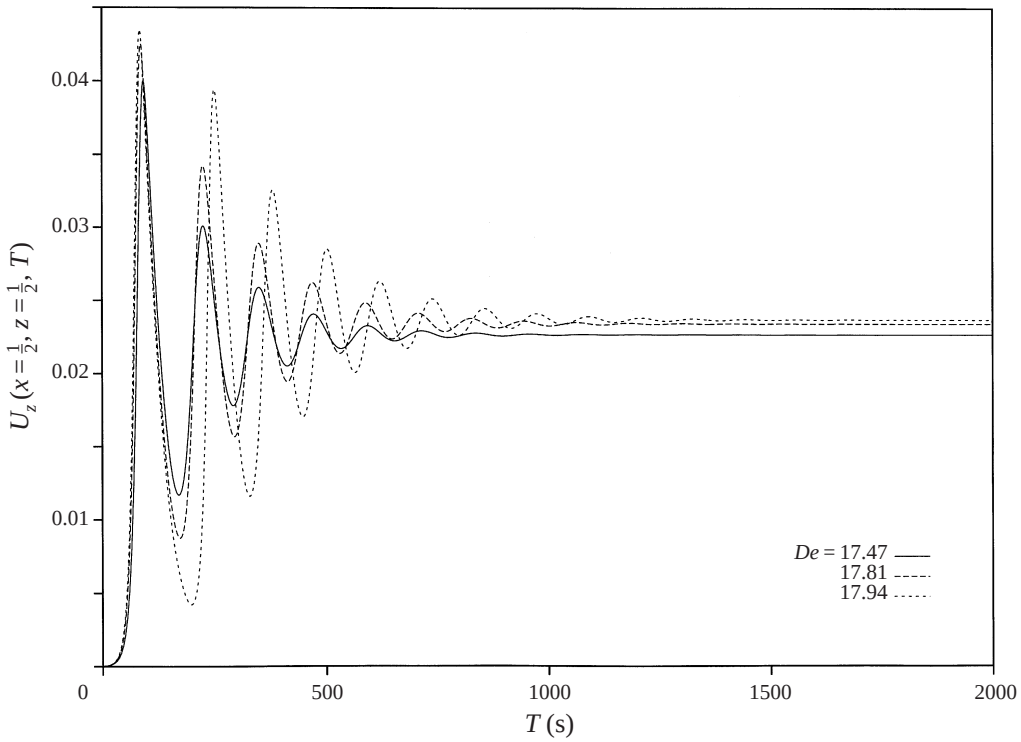

FIGURE 6. Oscillatory time evolution of the axial velocity for different shear rates ($17 < De < 18$) and small initial perturbation of the base flow. The parameters used are the same as in figure 4.

of Baumert & Muller (1995) for the low- and medium-viscosity fluids, corresponding most likely to $De < De_h$. However, they report the observation of coexistence of migrating bands and distorted vortices at the highest shear rate considered. Figure 7(*c*) shows the sequence of flow obtained for $De > De_h$. Avgousti *et al.* (1993) report having numerical difficulties for a UCM fluid when they take the slightly perturbed standing wave as their initial condition. Figure 7(*c*) shows the transition from steady to oscillatory TVF, and from one oscillatory level to the next. Additional theoretical and experimental investigations are obviously needed if the flow at still higher shear rate is to be explored. It is possible that the flow may not remain axisymmetric, a fact that does not seem to be suggested by the experiments of Baumert & Muller (1995).

4.2. *Weakly inertial flow and influence of boundary conditions*

The nonlinear behaviour is further examined through the influence of fluid elasticity in the presence of very weak inertial effects for the postcritical range of the Deborah numbers, in an attempt to recover the flow sequence observed in the experiment of Muller *et al.* (1993). Comparison between theory and experiment is expected to lead only to qualitative agreement given the relatively low number of normal stress modes in the 16NDS. A quantitative agreement is possible only if additional modes are included when inertia is completely neglected. The main objective of the present section is to compare the flows based on the RF and RR formulations.

Consider the flow with relatively small inertia, and set $Re = 0.004$. Also let $Rv = 3.75$ and $\varepsilon = 0.0625$ corresponding, respectively, to the viscosity ratio of the fluid and the gap-to-radius ratio used in the experiment (Muller *et al.* 1993). A more

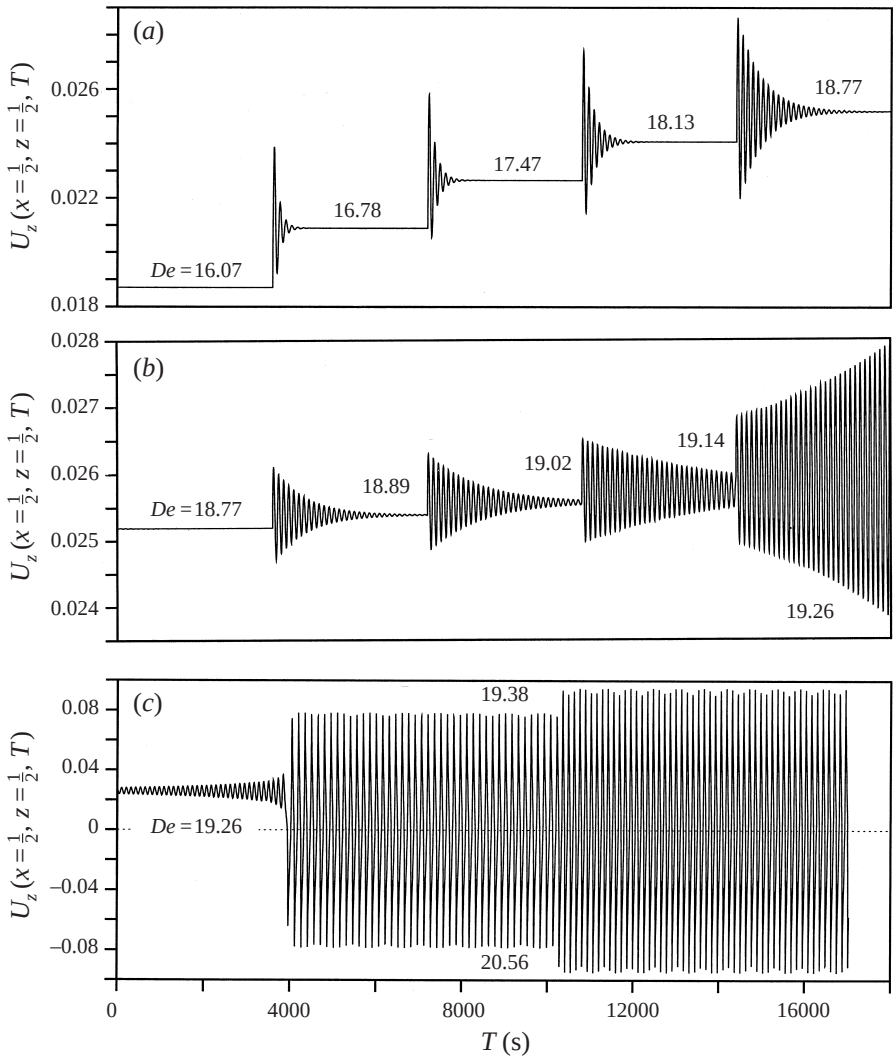

FIGURE 7. Time evolution of the axial velocity for $16 < De < 21$. The flow for each shear rate level is obtained using the flow of the previous (lower) level as initial conditions. The parameters used are the same as in figure 4. The figure is subdivided into three segments of 18 000 s period each. Steady TVF is always reached during the first period (*a*) for the range $16 < De < 18.7$. Oscillatory instability develops towards the end of the second period (*b*) for the range $18.6 < De < 19.27$. Transition to periodic behaviour occurs some time during the third period (*c*) for the range $19.26 < De < 21$.

detailed account of the experimental conditions and parameters is given in the next section. Although the wavenumber is not specified in the experiment, it is set equal to $k = 4$ based on wavenumbers reported in other experiments on TCF of viscoelastic fluids (Baumert & Muller 1995). Thus, only De will be varied. The flow is examined as De is increased from zero (Newtonian level). Referring to figure 3, it is seen that for $De = E = 0$ CF is unconditionally stable to any perturbation since $Re \ll 1$ in the present case. This situation remains practically unchanged until De reaches the theoretically predicted critical value, $De_c = 29.7$ or 29.3, depending on whether the RF or RR boundary conditions are used. These values are based on the purely elastic

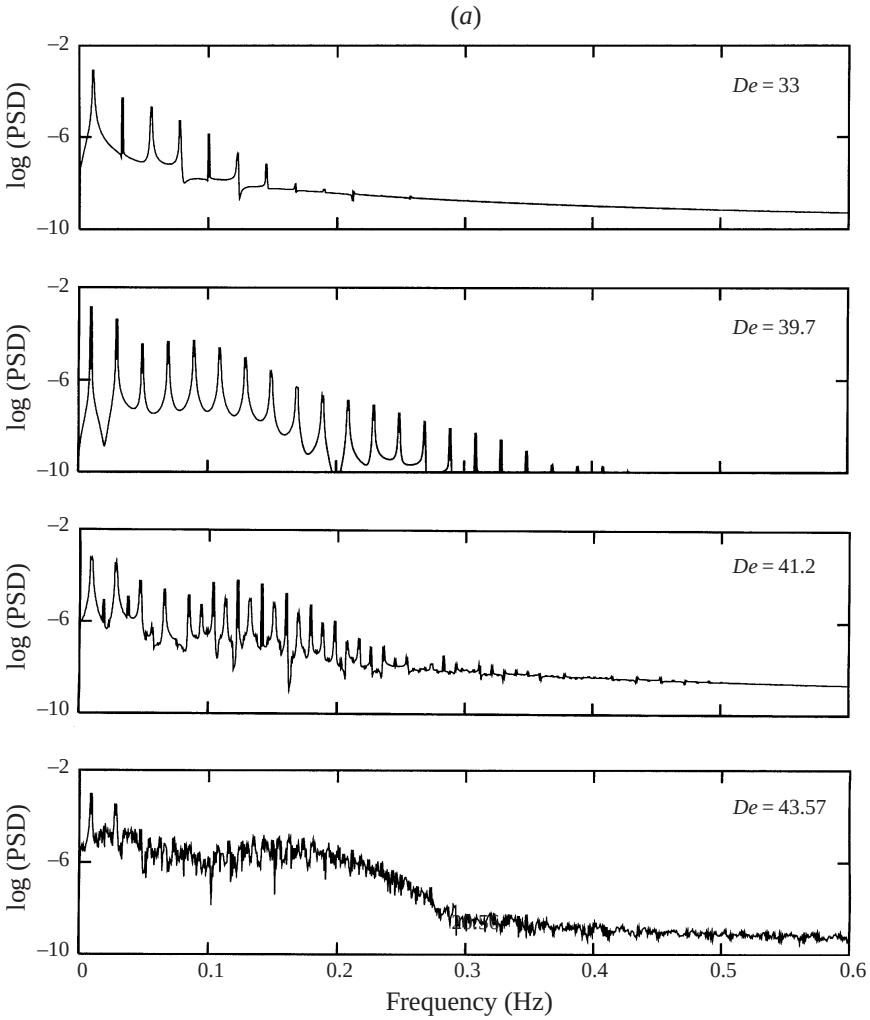

FIGURE 8 (*a*). For caption see facing page.

linear stability analysis. At this point, the base flow is supposed to lose its stability, but this is numerically detected at slightly higher De values. Since inertia effects are small ($Re = 0.004$), one observes an exchange of stability between the base flow and oscillatory TVF, since no steady TVF can set in the absence of inertia. As the Deborah number is increased beyond the critical value, the amplitude of oscillation increases. The resulting sequence of flows is identified through the Fourier spectra shown in figures 8(*a*) and 8(*b*) for the calculation based on the RF and RR boundary conditions, respectively. The range of Deborah numbers studied is the same as in the experiment: $32 < De < 53$, and should be compared with that reported in figures 7–10 of Muller *et al.* (1993), where it is noted that $De = 0.911 De_{Muller}$.

Theoretically, oscillatory TVF is expected to emerge at $De = 29.3$ for the RF formulation; in practice, however, it is detected at a higher Deborah number. At $De = 33$, the corresponding Fourier spectrum shown in figure 7(*a*) clearly displays periodic motion after the base flow becomes unstable. This periodic behaviour persists as De increases. The flow oscillates around the origin (CF), with amplitude that

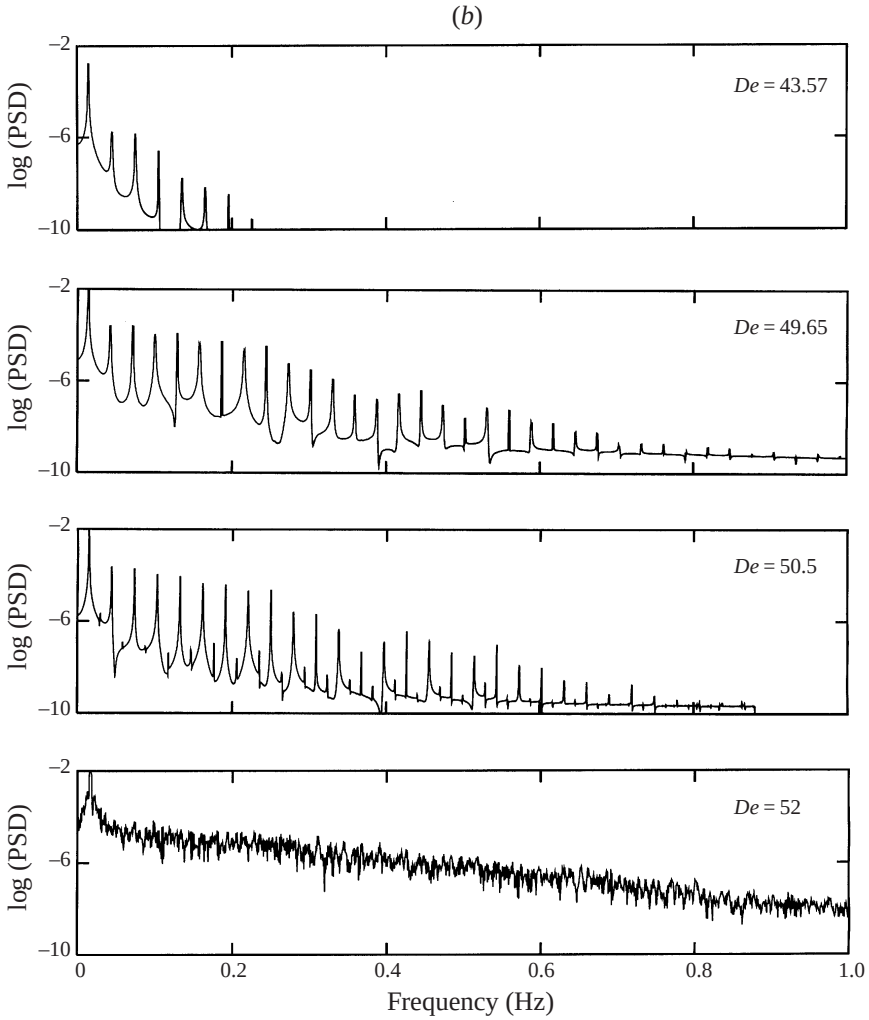

FIGURE 8. Highly elastic overstability for a Boger fluid ($Rv = 3.75$) with vanishingly weak inertia ($r = 10^{-6}$) and wavenumber $k = 4$. The Fourier spectrum in the postcritical range for (*a*) $De > De_c = 29.7$ based on the RF conditions, and (*b*) $De > De_c = 29.3$ based on the RR conditions.

increases as De increases. The spectrum shows the fundamental frequency and six odd harmonics. Additional harmonics emerge upon further increase of the Deborah number as shown for $De = 39.7$. Further increase in the elasticity level ($De = 41.2$) leads (most apparently) to a doubling in the period as depicted in the figure. It is not easy, in fact, to establish whether one is dealing with a bifurcation into period-2 motion or quasi-periodic behaviour on a torus. At $De = 43.57$, the power spectrum indicates clearly the presence of chaotic motion. A very similar sequence of flows is obtained on the basis of the RR formulation. The qualitative similarity is obvious from figure 7(*b*). Although the two formulations predict that the oscillatory TVF sets in at essentially the same critical Deborah number (29.3 vs. 29.7, for the RR and RF conditions, respectively), the emergence of higher harmonics, subharmonics and chaos occurs at higher De values for the RR formulations (figure 7*b*). This confirms, once again, that stick conditions tend to delay destabilization.

The sequence of flows predicted by the present model is clearly comparable to that reported by Muller *et al.* (1993). Experiment predicts a loss of stability of the origin at a critical Deborah equal to 32.3 while the present formulation gives $De_c = 29.7$. Direct quantitative comparison of the actual velocity amplitude is impossible since not all experimental parameters are available. It is possible that the experiment was in fact not conducted at fixed Reynolds number, and that De was increased by increasing Ω. Both theory and experiment predict the increase in amplitude of the velocity signal, the emergence of higher harmonics in the Fourier spectrum, and eventually that of subharmonics (corresponding to the onset of period doubling) as De increases.

4.3. *Purely elastic overstability and influence of higher-order modes*

The experimental measurements of Muller *et al.* (1993) were conducted under conditions of vanishingly small inertia. A close quantitative comparison between theory and experiment becomes possible when a modified twenty-mode dynamical system (20NDS) is used (Khayat 1997), which accounts for additional higher-order modes in the most influential normal stress components (that lead to the Weissenberg rod-climbing phenomenon). The model is thus adequate for the flow of a highly elastic fluid (with inertia neglected).

Not all the experimental flow parameters needed for the theory were explicitly reported in Muller *et al.* (1993). The test fluid used in the experiment has a (constant) viscosity $\eta = 162$ Pa s, and consists of 1000 p.p.m. high-molecular-weight polyisobutylene, dissolved in a viscous, low-molecular-weight polybutene of viscosity $\eta_s = 128$ Pa s. In this case, the solvent-to-polymer viscosity ratio $Rv = 3.76$. The fluid relaxation time, λ, varies depending on the rheological technique used to measure it. Steady shear flow data give $\lambda = 3.3$ s, while transient relaxation experiments lead to 10.9 s (Muller *et al.* 1993; Baumert & Muller 1995). In the calculations below, the value of λ is fixed by fitting one experimental point with theory. The inner and outer cylinder radii were 8 and 8.5 cm, respectively, so that $\varepsilon = 0.0625$. Although the inner cylinder angular velocity Ω was not explicitly given in the experiment, its value can be inferred from the range of experimental Deborah numbers $De_{Muller} = 2\Omega\lambda(1+\varepsilon)^2/[(1+\varepsilon)^2 - 1]$ used by Muller *et al.* (1993). Note that $De_{Muller}(\varepsilon \to 0) = De$ as defined in (4). It appears that there was only one fluid used throughout the experiment, and De_{Muller} was probably varied by varying only the inner cylinder speed, Ω. Hence, from the range of De_{Muller} values reported, the corresponding values of the inner cylinder speed is given by $\Omega = De_{Muller}/77.06$ for $\lambda = 4.4$ s. Muller *et al.* (1993) reported that the highest Reynolds number, Re, reached in the experiment was of the order 7×10^{-3}. Indeed, if one considers the value of Ω corresponding to the highest Deborah number reported ($De_{Muller} = 54.5$), one finds that $Re = 2.86 \times 10^{-3}$ (assuming the density $\rho \approx 1\,\mathrm{g\,cm^{-3}}$).

The experimental wavenumber, k, at which overstability is first observed, was also not reported by Muller *et al.* (1993); its measurement may have been difficult under transient conditions. Its exact value, however, is not crucial since De_c does not strongly depend on k. This is suggested by linear stability analysis and the flatness of the marginal stability curves around the minimum value of the critical Deborah number, over a wide range of practical values: $k \in [4, 8]$ for $Rv = 3.76$. The wavenumber is taken equal to $k_m = 4.85$, which corresponds to $De_c = De_c^m = 32$ as predicted by the linear stability analysis. This value is also close to wavenumbers reported in other experiments on TCF of viscoelastic fluids (Larson 1992). Thus, as in the experiment of Muller *et al.* (1993), only De will be varied (by varying Ω) in the following calculations and results.

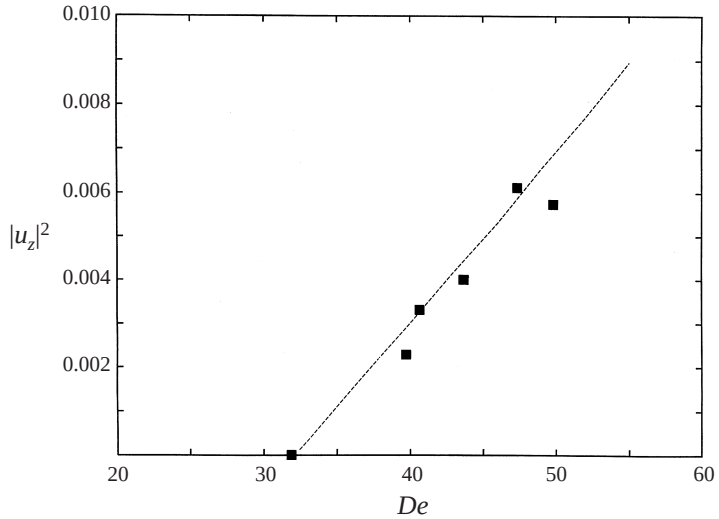

FIGURE 9. Bifurcation diagram and comparison between theory (dashed line) and experimental measurements (squares) of Muller *et al.* (1993). The figure shows the square of the amplitude of axial velocity at $x = \frac{1}{4}$ as a function of *De*.

Consider the flow as *De* is increased from zero (Newtonian level). Linear stability analysis indicates that CF is unconditionally stable for $De < 32$. In the absence of inertia, an exchange of stability takes place between CF and oscillatory TVF since no steady TVF can set in. The experimental critical value of the Deborah number at which oscillatory motion is first detected is equal to 32.3, and happens to be slightly larger than the theoretical value. As *De* is increased beyond the critical value, the amplitude of oscillation increases, confirming the existence and the stability of the Hopf bifurcation, in agreement with experiment. Calculations are carried out for the same range of Deborah numbers as in the experiment: $32 < De < 50$. At $De = 32.5$, the velocity signature and corresponding Fourier spectrum display periodic motion after CF becomes unstable. The amplitude of oscillation remains relatively small ($0.008\,\mathrm{cm\,s^{-1}}$). The power spectrum indicates the presence of a dominant frequency of 0.02 Hz and a weak second harmonics. This periodic behaviour persists as *De* increases, with the flow oscillating around the origin (CF). At $De = 43.57$, the motion remains periodic, with an increase in amplitude to $0.052\,\mathrm{cm\,s^{-1}}$. There is an increase in the fundamental frequency to 0.0298 Hz and the emergence of four significant even and odd harmonics. This trend persists as *De* is further increased with the eventual emergence of additional harmonics.

Figure 9 shows the Hopf bifurcation for the square of the velocity amplitude based on the twenty-mode model 20NDS, and the measurements from Muller *et al.* (1993). Both experiment and theory indicate that the amplitude of oscillation grows like $(De - De_c)^{1/2}$, in agreement with asymptotic analysis in the limit $De \to De_c$. Figure 10 displays the dependence of the dominant frequency and its harmonics on the Deborah number. The frequency tends to increase with *De* almost linearly. Unlike the amplitude, the frequency exhibits a jump at the critical Deborah number. This means that any initial weak velocity amplitude at the onset of oscillatory TVF has a dominant frequency that is relatively easy to detect. The agreement between the computed and measured frequencies is obvious from the figure. The apparent growing disagreement for the higher harmonics is to be expected. Any initial discrepancy at

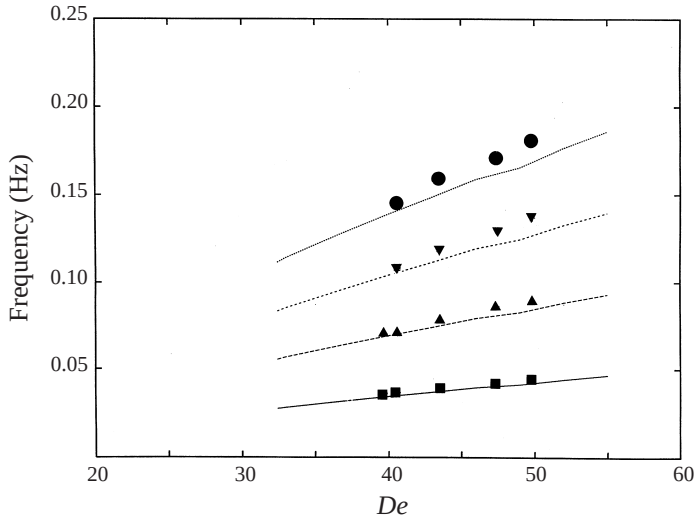

FIGURE 10. Frequency diagram and comparison between theory (continuous lines) and experimental measurements (symbols) of Muller *et al.* (1993).

the dominant frequency level is simply amplified as it is multiplied by two for the second harmonics, by three for the third harmonics and so on.

5. Discussion and concluding remarks

A dynamical system approach is proposed for the simulation of finite-amplitude TVF in the narrow-gap limit of a viscoelastic fluid of the Oldroyd-B type. This rather elementary Oldroyd-B constitutive model does not account for the rate-of-strain dependence of transport coefficients (viscosity and relaxation time), nor does it include the spectrum of relaxation times usually characteristic of polymeric fluids. However, this constitutive model is adopted in this study for at least four main reasons. First, since the aim of the study is to examine the influence of elasticity on the stability of TVF, the Oldroyd-B model does represent adequately highly elastic (Boger) fluids, for which the viscosity remains sensibly constant over a wide range of shear rates. A polyacrilamide solution in a maltose syrup/water mixture typically constitutes such a fluid (Walters 1980). Second, the Oldroyd-B constitutive equation is one of the simplest viscoelastic laws that accounts for normal stress effects (which lead to the Weissenberg rod-climbing phenomenon), which are responsible for the periodic phenomena arising in viscoelastic fluids. Other more realistic phenomenological or molecular-theory-based models (Bird *et al.* 1987; Tanner 1983) will likely lead to a different stability picture (Larson 1989). For instance, the presence of shear thinning, not accounted for by the Oldroyd-B equation, has a destabilizing effect since the effective Reynolds number increases as the viscosity decreases with increasing shear rate (Khayat 1996; Larson 1989). Third, the present formulation is a nonlinear stability analysis, which emphasizes the interplay between inertia and normal stress effects during the transition from CF to TVF. Nonlinear behaviour is reflected in the convective terms in the momentum equation and the upper-convective terms in the Oldroyd-B equation. Fourth, and most importantly, most experimental measurements and flow visualization so far reported on the TVF of viscoelastic fluids have been conducted on Boger fluids. Comparison between theory and experiment becomes

possible when the Oldroyd-B constitutive equation is used. However, only the inclusion of a distribution of relaxation times makes the constitutive model realistic.

The nonlinear dynamical system is derived by expanding the flow field in double Fourier series in space for the rigid–free (RF) boundary conditions, and Fourier/Chandrasekhar series for the rigid–rigid (RR) conditions. The set of ordinary differential equations, governing the time-dependent coefficients, is obtained after applying the Galerkin projection method, and adopting a suitable truncation to close the hierarchy of equations. The more severe truncation level used in the previous work (Khayat 1995*c*) led to a system (6NDS) derived by neglecting higher-order normal stresses terms. However, these terms tend to become significant for highly elastic flows or in the limit $Re \to 0$. The current 16NDS takes into account more effectively the influence of inertia and normal stresses; thus allowing direct comparison with the experiment of Baumert & Muller (1995). Good agreement was found, as the theory is capable of predicting conditions for monotonic and oscillatory transitions from CF and TVF. This also allows the assessment of the influence of the higher-order modes neglected previously, which are found to make a significant difference only for highly elastic fluids. The RF and RR boundary conditions lead essentially to the same qualitative stability and bifurcation pictures, and flow sequences of the transition to oscillatory TVF similar to the one observed by Muller *et al.* (1993). However, the RR conditions give much better agreement with experiment. An even better quantitative agreement with the experiment of Muller *et al.* (1993) was finally achieved when 20 modes were included (20NDS).

The close quantitative agreement between theory and experiment may be somewhat fortuitous given the uncertainty surrounding experimental parameters on the one hand, and the lack of a universal and accurate constitutive model for viscoelastic fluids on the other. Additional sources of discrepancy between theory and experiment are related to limitations of both Newtonian and viscoelastic flow formulations. The lack of a theory capable of predicting the value of the axial wavenumber, k, constitutes a major difficulty. The prediction of k remains an unresolved issue (in a given formulation, it is usually simply imposed from experimental observation). In the case of viscoelastic TCF, however, the measurement of k is difficult under transient flow conditions (Baumert & Muller 1995). Other parameters and variables are also difficult to obtain from the experiment of Muller *et al.* (1993) and had to be deduced. In particular, the relaxation time of the fluid can depend on the type of rheological device to measure it. In the calculations its value falls between two values reported by Muller *et al.* (1993) and was determined by forcing the theoretical curve to pass through one experimental point. Additional uncertainty originates from the type of constitutive model used. Although the Oldroyd-B equation predicts the behaviour of constant-viscosity highly elastic fluids, it does not incorporate the spectrum of relaxation times that is characteristic of real fluids. More complicated constitutive equations, accounting for the nonlinear dependence of the transport coefficients on the rate-of-strain tensor, can also be used within the framework of the present formulation. The Oldroyd-B model accounts only for nonlinearities stemming from the upper-convective terms in the constitutive equation. Another source of discrepancy may originate from end effects in the Taylor–Couette apparatus that have been neglected in the present formulation. The narrow-gap approximation is also a limiting assumption. Inertia effects can also play an influential role despite the fact that the experiment was conducted at a vanishingly small Reynolds number ($Re < 10^{-2}$). In general (Khayat 1995*a*), the presence of inertia, no matter how small it may be, prohibits the base flow from losing its stability to the overstable mode.

Instead, the base flow loses its stability first to steady (and not oscillatory) TVF since there is always a finite range of *Re* values over which the branches corresponding to steady TVF are stable.

Finally, the issue of non-axisymmetric modes is important; these modes are neglected in the present study. Linear stability analysis suggests that non-axisymmetric modes tend to be more unstable than axisymmetric modes, and it is only expected that their inclusion should make the formulation and results more realistic. One is then faced with the difficulty of finding the fully three-dimensional solution of a highly nonlinear problem, which, even in the limit of the Navier–Stokes equations, the Newtonian fluid community is still grappling with. More importantly, extensive experiments have been constantly suggesting that axisymmetric TVF of a viscoelastic fluid is always the one observed before non-axisymmetric WVF is observed. The agreement between the proposed axisymmetric theory and experiment seems to confirm this observation. However, it would be naïve to believe that the present study constitutes other than just the beginning or part of ongoing efforts to understand viscoelastic behaviour in the transition regime. In fact, the inclusion of non-axisymmetric modes would lead to worse agreement with experiment! This apparent paradox is due to the fact that, if non-axisymmetric modes are included, a more accurate constitutive model must also be used.

Let us first emphasize that all experimental studies on the TCF of polymeric fluids that we are aware of seem to indicate that, for a wide range of the Elasticity number *E*, (axisymmetric) TVF is always observed before the onset of (non-axisymmetric) WVF (Baumert & Muller 1995, 1999; Muller *et al.* 1993; Stock *et al.* 1992). Muller and coworkers have been conducting extensive experimental measurements and visualization on the TCF of polymeric solutions of low and high levels of elasticity, for the narrow and wide gaps. Their earlier findings indicate that: 'In the medium viscosity fluid, the lowest shear rate transitions were from the base flow to steady axisymmetric counter-rotating vortices; at moderate shear rates, the vortices are preceded by an oscillatory flow; at the highest rates examined, the vortices become stronger but more irregular... Under all conditions, the flow remained axisymmetric' (Baumert & Muller 1995). They also acknowledge that these observations are in contradiction with theoretical predictions, which indicate that non-axisymmetric disturbances are more dangerous than axisymmetric ones. However, Baumert & Muller (1995) insist that they consistently observe axisymmetric, rather than non-axisymmetric, disturbance flows. Also, examination of sequences of images of the gap captured at intervals of 1/30 s and longer did not reveal non-axisymmetry. Further, no waviness was apparent under ambient illumination.

Recently, Baumert & Muller (1999) confirmed their earlier observations by extending their experiments to the wide-gap TCF of two polymeric fluids. They concluded that as in the narrow-gap studies, in both fluids, the first transition from purely azimuthal base flow is always to an axisymmetric disturbance flow. This contradicts somewhat the observations of Groisman & Steinberg (1996, 1997) who reported that the first transition for highly elastic fluids is to disordered oscillations (or noisy, non-axisymmetric standing waves). However, Baumert & Muller remark that the first transition they observe is always to axisymmetric, counter-rotating vortices: they believe the discrepancy has to do with the extremely long onset and observation times required to observe the weak, axisymmetric flows reported in their experiment (Baumert & Muller 1999).

Then, where does the discrepancy between non-axisymmetric (linear) stability analysis and experiment come from? In other words: why does the axisymmetric theory

give better agreement with experiment? As mentioned earlier, the answer seems to lie mainly in the choice of an adequate constitutive viscoelastic model. The present and existing axisymmetric linear stability analyses, for a single-relaxation-time fluid, give a critical shear rate that corresponds closely to the experimental value. The non-axisymmetric analysis for the same fluid gives a critical shear rate 30–40% lower than the axisymmetric analysis. Larson *et al.* (1994) carried out axisymmetric linear stability analysis on a fluid with a distribution of relaxation times, and found that instabilities should occur at a shear rate higher than the experimental value. Thus, the inclusion of a spectrum of relaxation times tends to increase the value of the critical shear rate for instability, and the inclusion of non-axisymmetric modes tends to lower the critical shear rate. They attribute the good agreement between axisymmetric analysis and experiment to a 'partial cancellation of the two errors' induced by the neglect of non-axisymmetric modes and the inclusion of only one relaxation time in the constitutive model. This suggests that both non-axisymmetric modes and a more accurate constitutive model, which includes a spectrum of relaxation times, must be included to achieve an accurate formulation. At this time we are not aware of such a theory.

In conclusion, the current axisymmetric formulation demonstrates the usefulness of the low-dimensional approach in describing the complex phenomena arising from the interaction between inertia and elasticity in TCF. The study is the first attempt to lead to successful comparison and agreement with experiment. There is still no other theory that predicts (qualitatively or quantitatively) what is observed experimentally. Part of the reason for this lack of success may be the insistence of previous authors on seeking an 'exact' solution. Of course, higher-order modes in the solution representation, including non-axisymmetric modes, should eventually be included if a more accurate description is sought. However, even if a three-dimensional solution is found to the governing equations, there is no guarantee that it will lead to better agreement with experiment because of the uncertainty surrounding the constitutive equation. There is a lot of work that remains to be done: both non-axisymmetric modes and a spectrum of relaxation times for fluid behaviour must be included if a closer agreement with experiment is sought. However, the more accurate formulation may most likely confirm further the findings of Muller *et al.* that axisymmetric modes, and not non-axisymmetric modes, are the most dangerous modes.

The financial support of the Natural Sciences and Engineering Research Council is gratefully acknowledged. The author would also like to thank J. M. Floryan and A. Straatman for their helpful comments on the manuscript.

Appendix A. Solution expansion for the RF formulation (16NDS)

In this Appendix the Fourier modes used for the solution of (5)–(14) and the RF boundary conditions are listed for the velocity components, pressure and stress components. Only the two dominant modes are kept for each representation. Thus,

$$u_x(x,z,t) = \lfloor u_x^{11}(t)\sin(\pi x) + u_x^{12}(t)\sin(2\pi x)\rfloor \cos(kz), \tag{A 1}$$

$$u_y(x,z,t) = u_y^{01}(t)\sin(\pi x) + u_y^{02}(t)\sin(2\pi x) + \lfloor u_y^{11}(t)\sin(\pi x) + u_y^{12}(t)\sin(2\pi x)\rfloor \cos(kz), \tag{A 2}$$

$$u_z(x,z,t) = \lfloor u_z^{11}(t)\sin(\pi x) + u_z^{12}(t)\sin(2\pi x)\rfloor \sin(kz), \tag{A 3}$$

$$p(x,t) = \lfloor p_{11}(t)\cos(\pi x) + p_{12}(t)\cos(2\pi x)\rfloor \cos(kz); \tag{A 4}$$

$$\tau_{ii}(x,t) = \lfloor \tau_{ii}^{11}(t)\cos(\pi x) + \tau_{ii}^{12}(t)\cos(2\pi x)\rfloor \cos(kz), \quad i = x,y,z \text{ (no sum)}, \tag{A 5}$$

$$\tau_{xy}(x,t) = \tau_{xy}^{01}(t)\cos(\pi x) + \tau_{xy}^{02}(t)\cos(2\pi x) + \lfloor \tau_{xy}^{11}(t)\cos(\pi x) + \tau_{xy}^{12}(t)\cos(2\pi x)\rfloor \cos(kz), \tag{A 6}$$

$$\tau_{\alpha z}(x,t) = \lfloor \tau_{\alpha z}^{11}(t)\sin(\pi x) + \tau_{\alpha z}^{12}(t)\sin(2\pi x)\rfloor \sin(kz), \quad \alpha = x,y. \tag{A 7}$$

Appendix B. Solution expansion for the RR formulation (16NDS)

In this Appendix the Chandrasekhar modes used for the solution of (5)–(14) and the RR boundary conditions are listed for the velocity components, pressure and stress components. Only the two dominant modes are kept for each representation. Thus,

$$u_x(x,z,t) = \lfloor u_x^{11}(t)\Phi_1(x) + u_x^{12}(t)\Phi_2(x)\rfloor \cos(kz), \tag{B 1}$$

$$u_y(x,z,t) = u_y^{01}(t)\Phi_1(x) + u_y^{02}(t)\Phi_2(x) + \lfloor u_y^{11}(t)\Phi_1(x) + u_y^{12}(t)\Phi_2(x)\rfloor \cos(kz), \tag{B 2}$$

$$u_z(x,z,t) = \lfloor u_z^{11}(t)\Phi_1'(x) + u_z^{12}(t)\Phi_2'(x)\rfloor \sin(kz), \tag{B 3}$$

$$p(x,t) = \lfloor p_{11}(t)\Phi_1'(x) + p_{12}(t)\Phi_2'(x)\rfloor \cos(kz); \tag{B 4}$$

$$\tau_{ii}(x,t) = \lfloor \tau_{ii}^{11}(t)\cos(\pi x) + \tau_{ii}^{12}(t)\cos(2\pi x)\rfloor \cos(kz), \quad i = x,y,z \text{ (no sum)}, \tag{B 5}$$

$$\tau_{xy}(x,t) = \tau_{xy}^{01}(t)\Phi_1'(x) + \tau_{xy}^{02}(t)\Phi_2'(x) + \lfloor \tau_{xy}^{11}(t)\Phi_1'(x) + \tau_{xy}^{12}(t)\Phi_2'(x)\rfloor \cos(kz), \tag{B 6}$$

$$\tau_{\alpha z}(x,t) = \lfloor \tau_{\alpha z}^{11}(t)\Phi_1(x) + \tau_{\alpha z}^{12}(t)\Phi_2(x)\rfloor \sin(kz), \quad \alpha = x,y, \tag{B 7}$$

where $\Phi_1(x)$ and $\Phi_2(x)$ are, respectively, the even and odd Chandrasekhar functions given by (Chandrasekhar 1961)

$$\Phi_1(x) = \frac{\cosh(\lambda x)}{\cosh(\lambda/2)} - \frac{\cos(\lambda x)}{\cos(\lambda/2)}; \quad \Phi_2(x) = \frac{\sinh(\mu x)}{\sinh(\mu/2)} - \frac{\sin(\mu x)}{\sin(\mu/2)}. \tag{B 8}$$

The condition of orthogonality and the no-slip boundary conditions lead to the following equations for the constants λ and μ:

$$\tanh(\lambda/2) + \tan(\lambda/2) = \coth(\mu/2) - \cot(\mu/2) = 0. \tag{B 9}$$

The functions $\Phi_1'(x)$ and $\Phi_2'(x)$ are defined by

$$\Phi_1'(x) = \frac{\sinh(\lambda x)}{\cosh(\lambda/2)} + \frac{\sin(\lambda x)}{\cos(\lambda/2)}; \quad \Phi_2'(x) = \frac{\cosh(\mu x)}{\sinh(\mu/2)} - \frac{\cos(\mu x)}{\sin(\mu/2)}. \tag{B 10}$$

Note that the range of x values is, for convenience, taken to be $[-\frac{1}{2}, +\frac{1}{2}]$ instead of the range $[0, +1]$ used in the main text.

REFERENCES

Ashrafi, N. & Khayat, R. E. 1999 A low-dimensional approach to nonlinear plane-Couette flow of viscoelastic fluids. *Phys. Fluids* (in press).

Avgousti, M. & Beris, A. N. 1993 Non-axisymmetric modes in viscoelastic Taylor–Couette flow. *J. Non-Newtonian Fluid Mech.* **50**, 225.

Avgousti, M., Liu, B. & Beris, A. N. 1993 Spectral methods for the viscoelastic time-dependent flow equations with applications to Taylor–Couette flow. *Intl J. Numer. Meth. Fluids* **17**, 49.

Baumert, B. M. & Muller, S. J. 1995 Flow visualization of the elastic Taylor–Couette flow in Boger fluids. *Rheol. Acta* **34**, 147.

Baumert, B. M. & Muller, S. J. 1999 Axisymmetric and non-axisymmetric elastic and inertio-elastic instabilities in Taylor–Couette flow. *J. Non-Newtonian Fluid Mech.* **83**, 33.

Bird, R. B., Armstrong, R. C. & Hassager, O. 1987 *Dynamics of Polymeric Liquids*, vol. 1, 2nd Edn. John Wiley & Sons.

Chandrasekhar, S. 1961 *Hydrodynamic and Magnetohydrodynamic Stability*. Dover.

Davey, A. 1962 The growth of Taylor vortices between rotating cylinders. *J. Fluid Mech.* **14**, 336.

Drazin, P. G. & Reid, W. H. 1981 *Hydrodynamic Stability*. Cambridge University Press.

Groisman, A. & Steinberg, V. 1996 Couette–Taylor flow in a dilute polymer solution. *Phys. Rev. Lett*. **77**, 1480.

Groisman, A. & Steinberg, V. 1997 Solitary vortex pairs in viscoelastic Couette flow. *Phys. Rev. Lett*. **78**, 1460.

Joo, Y. L. & Shaqfeh, E. S. G. 1992 The effect of inertia on the viscoelastic Dean and Taylor–Couette flow instabilities with application to coating flows. *Phys. Fluids* A **4**, 2415.

Khayat, R. E. 1994 Chaos and overstability in the thermal convection of viscoelastic fluids. *J. Non-Newtonian Fluid Mech.* **53**, 227.

Khayat, R. E. 1995*a* Nonlinear overstability in the thermal convection of viscoelastic fluids. *J. Non-Newtonian Fluid Mech.* **58**, 331.

Khayat, R. E. 1995*b* Fluid elasticity and the onset of chaos in thermal convection. *Phys. Rev*. E **51**, 380.

Khayat, R. E. 1995*c* Onset of Taylor vortices and chaos in viscoelastic fluids. *Phys. Fluids* A **7**, 2191.

Khayat, R. E. 1996 Onset of chaos in the thermal convection of weakly shear thinning fluids. *J. Non-Newtonian Fluid Mech.* **63**, 153.

Khayat, R. E. 1997 Low-dimensional approach to nonlinear overstability of purely elastic Taylor-vortex flow. *Phys. Rev. Lett*. **78**, 4918.

Kuhlmann, H. 1985 Model for Taylor–Couette flow. *Phys. Rev*. A **32**, 1703.

Kuhlmann, H., Roth, D. & Lücke, M. 1988 Taylor flow and harmonic modulation of the driving force. *Phys. Rev*. A **39**, 745.

Larson, R. G. 1989 Taylor–Couette stability analysis for a Doi–Edwards fluid. *Rheol. Acta* **28**, 504.

Larson, R. G. 1992 Instabilities in viscoelastic flows. *Rheol. Acta* **31**, 213.

Larson, R. G., Muller, S. J. & Shaqfeh, E. S. G. 1994 The effect of fluid rheology on the elastic Taylor–Couette instability. *J. Non-Newtonian Fluid Mech.* **51**, 195.

Larson, R. G., Shaqfeh, E. S. G. & Muller, S. J. 1990 A purely elastic instability in Taylor–Couette flow. *J. Fluid Mech.* **218**, 573.

Marcus, P. S. 1984 Simulation of Taylor–Couette flow. Part 2. Numerical results for wavy-vortex flow with one travelling wave. *J. Fluid Mech.* **146**, 65.

McLaughlin, J. B. & Martin, P. C. 1975 Transition to turbulence in a statically stressed fluid system. *Phys. Rev*. A **12**, 186.

Muller, S. J., Shaqfeh, E. S. J. & Larson, R. G. 1993 Experimental study of the onset of oscillatory instability in viscoelastic Taylor–Couette flow. *J. Non-Newtonian Fluid Mech.* **46**, 315.

Normand, C. & Pomeau, Y. 1977 Convective instability: a physicist approach. *Rev. Mod. Phys.* **49**, 581.

Northey, P. J., Armstrong, R. C. & Brown, R. A. 1992 Finite-amplitude time-periodic states in viscoelastic Taylor–Couette flow described by the UCM model. *J. Non-Newtonian Fluid Mech.* **42**, 117.

Sell, G. R., Foias, C. & Temam, R. 1993 *Turbulence in Fluid Flows: A Dynamical Systems Approach*. Springer.

Shaqfeh, E. S. G. 1996 Purely elastic instabilities in viscoelastic flows. *Ann. Rev. Fluid Mech.* **28**, 129.

Shaqfeh, E. S. G., Muller, S. J. & Larson, R. G. 1992 The effect of gap width and dilute solution properties on the viscoelastic Taylor–Couette instabilities. *J. Fluid Mech.* **235**, 285.

Shirer, H. N. & Wells, R. 1980 *Mathematical Structure of the Singularities at the Transitions Between Steady States in Hydrodynamic Systems*. Springer.

Sparrow, C. 1983 *The Lorenz Equations*. Springer.

Stock, H., Zisenis, M., Cleschinsy, D. & Springer, J. 1992 Analysis of Taylor vortex flow by means of laser light scattering. *Rheol. Acta* **31**, 274.

Stuart, J. T. 1958 On the nonlinear mechanics of hydrodynamic stability. *J. Fluid Mech.* **4**, 1.

Sureshkumar, R., Beris, A. N. & Avgousti, M. 1994 Non-axisymmetric subcritical bifurcations in viscoelastic Taylor–Couette flow. *Proc. R. Soc. Lond.* A **447**, 135.

Tanner, R. I. 1983 *Engineering Rheology*. Oxford University Press.

Veronis, G. 1966 Motions at subcritical values of the Rayleigh number in a rotating fluid. *J. Fluid Mech.* **24**, 545.

Walters, K. 1980 *Rheometry: Industrial Applications.* Research Studies Press.